THE JOURNAL OF PHYSICAL CHEMISTRY B

ARTICLE

pubs.acs.org/JPCB

Electroporation of the *E. coli* and *S. Aureus* Membranes: Molecular Dynamics Simulations of Complex Bacterial Membranes

Thomas J. Piggot, Daniel A. Holdbrook, and Syma Khalid*

School of Chemistry, University of Southampton, Highfield, Southampton SO17 1BJ, United Kingdom

Supporting Information

ABSTRACT: Bacterial membranes are complex organelles composed of a variety of lipid types. The differences in their composition are a key factor in determining their relative permeabilities. The success of antibacterial agents depends upon their interaction with bacterial membranes, yet little is known about the molecular-level interactions within membranes of different bacterial species. To address this, we have performed molecular dynamics simulations of two bacterial membranes: the outer membrane of *E. coli* and the cell membrane of *S. aureus*. We have retained the chemical complexity of the membranes by considering the details of their lipidic components. We identify the extended network of lipid−lipid interactions that stabilize the membranes. Our simulations of electroporation show that the *S. aureus* cell membrane is less resistant to poration than the *E. coli* outer membrane. The mechanisms of poration for the two membranes have subtle differences; for the *E. coli* outer membrane, relative differences in mobilities of the lipids of both leaflets are key in the process of poration.

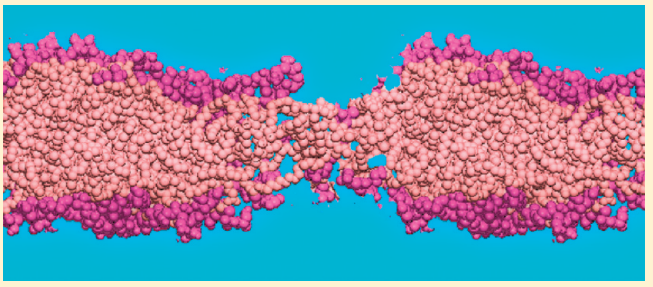

INTRODUCTION

A feature common to all bacterial cells is the presence of a lipid membrane that defines the boundary between the inside of the cell and the extracellular environment. These cellular barriers allow the regulation of the intracellular environment, a process that is essential for the correct functioning and survival of the cells. Bacterial species can differ substantially in the composition of their membranes; it is thought that the composition of the membrane plays a key role in its permeability properties.

Gram-negative bacteria, of which *E. coli* is an archetypal example, are unique in terms of membrane composition; they are surrounded by two membranes that are separated by the periplasmic space.[1] The inner membrane is a phospholipid bilayer with a relatively simple lipid composition. In contrast, the outer membrane (OM) is an asymmetric bilayer; the inner leaflet is composed of phospholipids while the outer leaflet is composed of lipopolysaccharide (LPS).[2,3] The composition of this membrane renders it impermeable to hydrophobic and large polar molecules.[4,5] The outer membrane is also thought to play a role in the correct folding and assembly of the proteins that reside with it.[6,7]

In contrast to the double-membrane cell wall structure of Gram-negative bacteria, Gram-positive bacteria are surrounded by a single cell membrane. Similarly to the inner leaflet of the Gram-negative OM, this membrane is composed of phospholipids. *S. aureus*, a Gram-positive bacterium that commonly colonises human skin, is known to cause severe disease and even mortality especially in patients who have undergone surgical procedures.[8] The membrane of *S. aureus* contains a substantial proportion of an unusual phospholipid called lysyl-phosphatidylglycerol (Lys-PG).[9] In contrast to most other, more commonly found natural phospholipids, which are either neutral (e.g., phosphatidylcholine (PC) and phosphatidylethanolamine (PE)) or negatively charged (e.g., phosphatidylglycerol (PG) and phosphatidylserine), Lys-PG is positively charged. The positive charge confers unique characteristics to the *S. aureus* membrane, including resistance to the membrane disrupting properties of cationic antimicrobial peptides,[10,11] although the molecular mechanisms through which resistance to antimicrobials develops, remain to be determined.

From a therapeutic perspective, crossing the membrane to gain entry into bacterial cells is of fundamental importance, for example, for antibiotic drugs. The composition of a particular membrane in terms of its lipidic content is considered to play a key role in the permeability properties of the membrane, therefore, it is important to characterize the molecular interactions within these membranes that stabilize them and impart their characteristic properties.

While some drugs are small hydrophobic molecules and thus are able to diffuse freely across membranes, the membranes of both Gram-positive and Gram-negative bacteria are impermeable to diffusion of larger molecules. Electroporation is commonly employed to provide a route for these larger molecules to cross bacterial membranes in vitro. An external electric field is applied across the membrane to induce pore formation through which molecules are able to pass into the cells. Several previously reported studies have described molecular dynamics (MD) simulations of electroporation of simple membranes have shown

Received: July 22, 2011
Revised: October 4, 2011
Published: October 04, 2011

that the process of electroporation proceeds via the initial formation of a single-file water channel. This water channel is stabilized through interactions with lipid head groups, which subsequently move into the membrane core.[12−18] While some of these simulations have moved beyond simple representations of the membrane (e.g., by including some asymmetry and charged lipids, etc.[19,20]), the lipid compositions of bacterial membranes have not been addressed. Thus, despite being a commonly used technique, the detailed molecular mechanisms of the poration process, especially for complex membranes, have not been well-characterized. Similarly, while atomistic simulations of outer membrane proteins have provided a wealth of information regarding the dynamics of the proteins, they have tended to include relatively simple models of the lipidic membrane components.[21−24] The simulations of the *P. aeruginosa* outer membranes reported by Straatsma and co-workers[25−28] were the first to incorporate the asymmetry of the bacterial outer membrane, however, a simple model of the inner leaflet was used.

In the following, we employ atomistic molecular dynamics simulations to describe the molecular interactions within the membranes of *E. coli* and *S. aureus* (Figure 1). The molecular mechanisms of electroporation of the two membranes are probed through a series of simulations performed at differing applied electric field strengths. In particular, we are able to identify key differences in the behavior of the Gram-negative outer membrane compared to the Gram-positive membrane under an applied electric field. Our model of the *E. coli* outer membrane (EcOM) incorporates the complex LPS in the outer leaflet and a realistic mixture of phospholipids in the inner leaflet, while the *S. aureus* cell membrane (SaCM) also includes representative ratios of the component lipids, thus, the chemical complexity is retained. The models of the SaCM and EcOM described here, represent the most complex (in terms of composition) models reported to date.

METHODS

Simulation Systems. A summary of both simulation system components is provided in Table 1. The phospholipid composition of the SaCM in the simulations was 54% PG, 36% Lys-PG, and 5% diphosphatidylglycerol (DPG; also known as Cardiolipin), in close agreement to the experimentally determined compositions from *S. aureus*.[9,29] The fatty acyl tails of the SaCM phospholipids were all 15 carbon anteiso-branched (15-*a*) chains, which are the most common lipid tails found in the SaCM.[9,30] Details of the initial SaCM bilayer construction are provided in the Supporting Information.

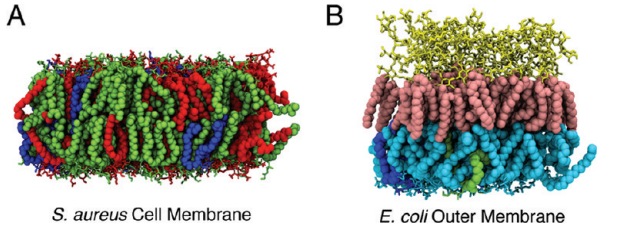

Figure 1. Snapshots of (A) the *S. aureus* cell membrane and (B) *E. coli* outer membrane models. PG lipids are shown in green, Lys-PG red, DPG blue, and PE cyan. LPS lipid tails are shown in pink and LPS sugars in yellow.

The outer leaflet of the EcOM bilayer was composed entirely of Rd_1 LPS molecules, which comprises lipid A and the inner core of the LPS.[5] The inner core used for the Rd_1 LPS was from the R1 core type,[31] the most common core composition in *E. coli*.[32] The inner leaflet of the membrane was composed of a mixture of PE (90%), PG (5%), and DPG (5%) phospholipids.[33] The phospholipid fatty acyl tail composition of the inner leaflet was (1-palmitoly, 2-*cis*-vaccenyl (PV) for PE and PG, and 1-palmitoyl, 2-*cis*-vaccenyl, 3-pamitoly, 4-*cis*-vaccenyl (PVPV) for DPG. Details of the construction of the asymmetric EcOM are provided in the Supporting Information. Lipid parameter details and validations are also provided in the Supporting Information.

Simulation Protocols. All simulations were performed using the GROMACS package,[34−36] version 4.5.1, the GROMOS 53A6 force field[37] and the SPC water model.[38] During the simulations the LPS, phospholipids and solvent (water plus ions) were maintained at a constant temperature above the gel (L_β) to liquid crystal (L_α) phase transition temperatures[39−44] using the Nosé-Hoover thermostat with a time constant of 0.5 ps.[45,46] A pressure of 1 bar was maintained using anisotropic pressure coupling with the Parrinello-Rhaman barostat and a time constant of 5 ps.[47,48] Electrostatic interactions were treated using the smooth particle mesh Ewald (PME) algorithm[49] with a short-range cutoff of 0.9 nm. The van der Waals interactions were truncated at 1.4 nm with a long-range dispersion correction applied to the energy and pressure. The neighbor list was updated every five steps during the simulations. All bonds were constrained using the LINCS algorithm[50] allowing a 2 fs time step to be applied. These simulation parameters were chosen so as to replicate those used in the work of Kukol[51] from which the phospholipid parameters used in these simulations were originally based. SaCM and EcOM bilayers were simulated for 200 ns, a repeat simulation with different initial velocities was performed for each bilayer to ensure reproducibility.

Electroporation Simulations. In these simulations a constant external electric field was applied to both the SaCM and EcOM bilayers, parallel to the bilayer normal, at the three different electric field strengths of 0.3, 0.4, and 0.5 V/nm. The EcOM was also simulated under electric field strengths of 0.4 and 0.5 V/nm applied with a reversed polarity. Simulations were performed for 200 ns or until the systems collapsed due to poration of the membranes. In the same approach to that taken by Böckmann et al.,[17] structures were taken from the simulations after initial pore formations and simulated for 50−100 ns at a lower field strengths of 0.04 V/nm, and for the EcOM also at 0.08 V/nm, to study the properties of the pores without a collapse of the membranes.

Table 1. Lipid Compositions and Simulation Details of the Equilibrium Simulations

system	number of lipids					solvent	simulation length (ns)
	Rd_1 LPS	PE	PG	DPG	Lys-PG		
E. coli outer membrane (outer leaflet)	64					332 Mg^{2+}25436 H_20	2 × 200
E. coli outer membrane (inner leaflet)		144	8	8			
S. aureus cell membrane			108	10	72	56 Na^+11930 H_20	2 × 200

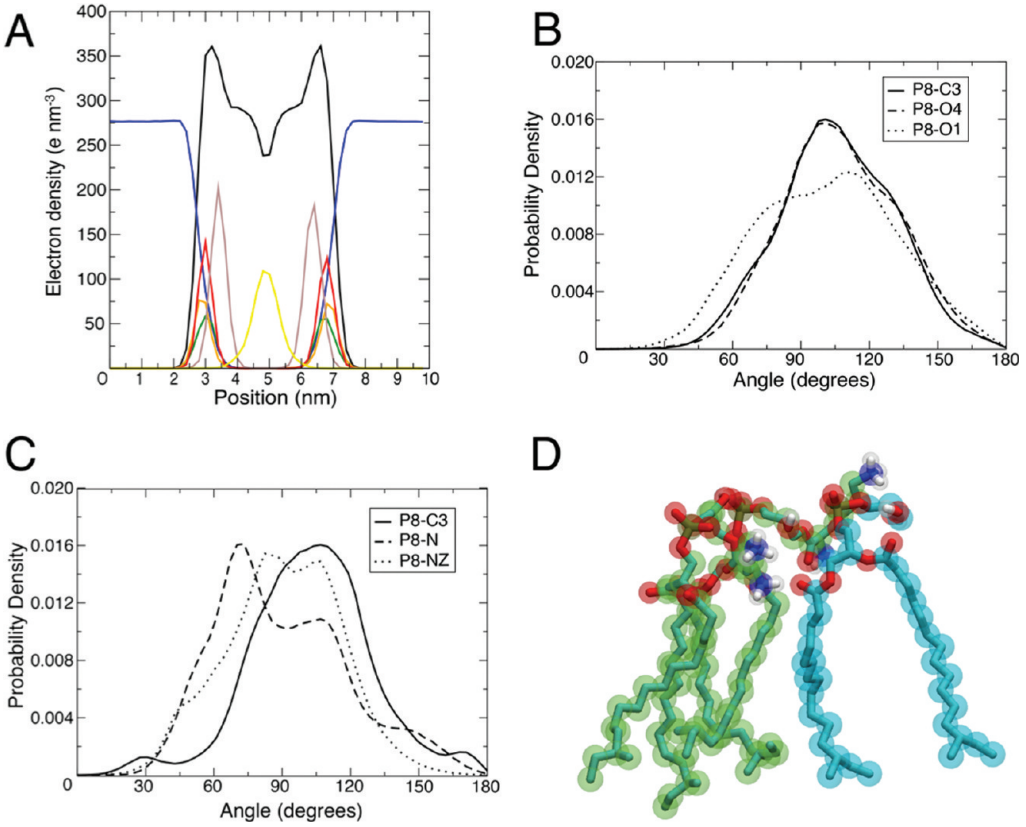

Figure 2. Equilibrium properties of the SaCM. (A) The electron density profile (black, lipids; blue, water; green, lysine of the Lys-PG; orange, glycerol headgroup; red, phosphate; brown, carbonyl groups; yellow, methyl). (B) PG and (C) Lys-PG headgroup angles with respect to the bilayer normal. A value of zero would mean that the angle is pointing toward the center of the bilayer. (D) A picture showing the network of hydrogen bond interactions for three lipids in the SaCM.

RESULTS

Model Membrane Simulations. To perform accurate simulations of the complex membranes studied in this work, it is essential that the individual components of the membranes sufficiently reproduce experimentally determined properties of these membrane components. Results of simulations, performed for PG, PE, Lys-PG, and DPG bilayers, can be found in the Supporting Information and show that the parameters used in these simulations accurately reproduce experimental properties of these membrane components.

***E. coli* and *S. aureus* Membrane Dynamics.** Our models retain the natural complexity of the in vivo membranes in terms of their chemical composition and, therefore, provide a route to studying the intramembrane, molecular interactions that stabilize the membranes. Thus, it is useful to discuss the equilibrium properties of the bilayers before considering electroporation events.

S. aureus Cell Membrane. One of the most frequently analyzed physical properties from MD simulations of lipid membranes is the area per lipid or area per acyl chain (A_C). While this property is difficult to determine experimentally,[52] it does provide a metric for comparison with other simulations and also a route to determining if the system has equilibrated. The A_C of the SaCMs during the 200 ns simulations are shown in Supporting Information, Figure S4. The A_C reached an equilibrium value after ~100 ns of simulation. During the last 100 ns of simulations, the average value of A_C was 0.309 nm^2 (± 0.003 nm^2). The A_C is higher than would be expected for the unbranched DPPG and Lys-DPPG lipids at this temperature (313 K). The higher A_C is presumably due to the presence of the anteiso-branched methyl groups in the lipid tails, as has been observed for other branched lipids.[53]

The interactions between lipids are key to the physicochemical properties of the membrane and hence its biological function. To explore these quantitatively, we first sought to determine the location of the various chemical components of the lipids, by calculating the electron density profile of the SaCM membrane (Figure 2A). Interestingly, the peaks corresponding to both lysine and glycerol groups of the D(15-*a*)Lys-PG headgroup partially overlap with the lipid phosphate peak, although the lysine group is on average ~0.1−0.2 nm closer to the center of the bilayer than the glycerol headgroup. The location of this lysine group is somewhat unexpected due to the large size of the Lys-PG headgroup. The orientations of the head groups of D(15-*a*)PG and D(15-*a*)Lys-PG were evaluated via calculation of the angles of the P8-C3, P8-O1, and P8-O4 (Figure 2B, PG) or P8-C3, P8-N, and P8-NZ (Figure 2C, Lys-PG) vectors with respect to the bilayer normal for each lipid during the final 100 ns of the simulation (see Supporting Information, Figure S5 for lipid atom naming conventions). Both the PG and Lys-PG head groups, on average, lie approximately parallel to the bilayer surface. For PG the P8−C3, P8−O1, and P8−O4 angles are 104.4° (±2.5°), 99.9° (±3.0°), and 105.7° (±2.5°), respectively. This indicates that the PG headgroup has a more vertical orientation relative to the surface of the bilayer. For Lys-PG, the P8−N angle displays a bimodal distribution with a major peak at ~72° and a minor peak

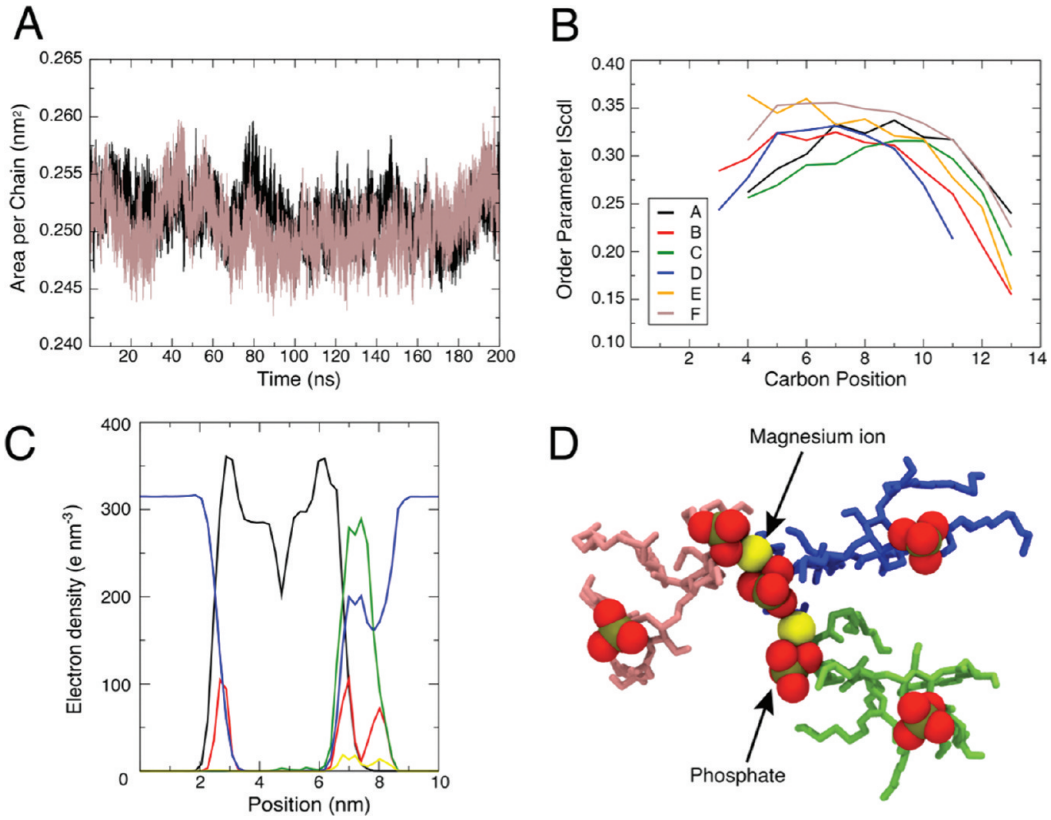

Figure 3. Equilibrium properties of the EcOM. (A) The A_C during the EcOM simulations. (B) The deuterium order parameters of the acyl chains of the LPS during the simulation. (C) The electron density profile of the EcOM (black, phospholipid and lipid A; blue, water; green, inner core; red, phosphate; yellow, magnesium ions). (D) A snapshot showing two magnesium ions cross-linking three LPS molecules. The inner core sugars have been omitted for clarity.

at ~107°, while the P8−NZ and P8−C3 angles are on average 88.7° (±2.5°) and 101.2° (±2.7°), respectively. The respective orientations of the lipids enable stabilizing interlipid hydrogen bonding interactions. For PG, the majority of the interactions from the glycerol headgroup are for the O4−H5 group, intermolecular hydrogen bonds to PG and Lys-PG phosphate groups (occurring, on average, for 20.63 and 14.26% of the simulations, respectively). For the O1−H0 group this intermolecular hydrogen bond to phosphate groups is also observed. In addition there is also the formation of an intramolecular hydrogen bond from O1−H0 to the PG phosphate group, for on average 18.33% of the time in the simulations. For Lys-PG this O4−H5 intermolecular hydrogen bond is also formed to phosphate groups. Both ammonia groups in the lysine region of the headgroup form intra- and intermolecular hydrogen bonds to phosphate and more commonly carbonyl ester groups of the lipids (see Table S6 for the details of these interactions). An example of the complex network of hydrogen bonding interactions in the SaCM is provided in Figure 2D. Additional stabilizing interactions within the SaCM come from electrostatic interactions between lipids and Na^+ ions. The Na^+ ions preferentially bind to the carbonyl oxygen atoms of the lipids (see Supporting Information, Figure S6A). Cross-linking interactions between one Na^+ ion and more than one lipid molecule were a common feature of the SaCM membrane. An example of this ion mediated lipid interaction is shown in Supporting Information, Figure S6B. These interactions are similar to those observed in PG bilayer simulations.[51,54]

E. coli Outer Membrane. There was little deviation in the A_C for the Rd_1 LPS during the course of the simulation, confirming this layer had been sufficiently pre-equilibrated. During the final 100 ns of the EcOM simulations (Figure 3A), the A_C for the Rd_1 LPS was 0.251 nm^2 (±0.002 nm^2). This is in good agreement with the experimental estimate of 0.260 nm^2 for the upper limit of the A_C of the LPS.[55]

The electron density profile of the EcOM (Figure 3C) shows the ordered nature of the LPS outer leaflet. The headgroup-to-headgroup thickness (D_{HH}) of the membrane, calculated from the electron density, is 3.29 nm. This is in good agreement with predictions made from the hydrophobic thickness of outer membrane proteins based upon the two rings of aromatic residues located at the membrane interfaces (e.g., for OmpF[56]) given the differences in D_{HH} and hydrophobic thickness.[57] The electron density profile shows close association of magnesium ions with phosphate groups of the Rd_1 LPS. Interaction of Mg^{2+} ions with multiple phosphate groups enables cross-linking of LPS molecules leading to an extended network of electrostatic interactions (Figure 3D). Similar cross-linking has been reported from simulations of the *P. aeruginosa* outer membrane.[25] Furthermore, these observations are consistent with experimental studies of the interaction of divalent cations and LPS.[42] Hydrogen bond interactions are also formed within, and between Rd_1 LPS molecules. The hydroxyl, carboxylate and phosphate groups of the LPS inner core sugars are involved in this network of inter and intramolecular hydrogen bond interactions, as shown in Supporting Information, Figures S6C and S6D.

Table 2. Lipid Diffusion Coefficients from the Equilibrium Simulations

lipid	diffusion coefficient (10^{-8} cm^2/s)
Rd_1 LPS	0.133 (±0.023)
PVPE	3.252 (±0.122)
D(15-*a*)PG	1.187 (±0.243)
D(15-*a*)Lys-PG	0.921 (±0.046)

Table 3. Electroporation Simulations and the Time Scales of Pore Formation

system	field strength[a] (V/nm)	pore formation time[b] (ns)
E. coli outer membrane	0.3	no pore in 200 ns
		no pore in 200 ns
	0.4	53.50
		31.80
	−0.4	40.75
	0.5	6.45
		5.60
	−0.5	4.40
S. aureus cell membrane	0.3	149.05
		95.85
	0.4	24.65
		13.80
	0.5	7.60
		9.05

[a] A negative number indicates the electric field was applied with reversed polarity. [b] Time taken for the formation of a hydrophilic pore.

When considering the permeability of bacterial membranes, it is useful to characterize their dynamic properties by evaluating the mobility of the lipids within the monolayers. To address this we have calculated the diffusion coefficients of the lipids in the EcOM (Table 2). The diffusion coefficient of the Rd_1 LPS molecules is 0.133 (± 0.023) × 10^{-8} cm^2/s. This diffusion coefficient is in good agreement with the experimentally determined value for the diffusion of LPS.[58] In comparison, as expected, the diffusion rate of the inner leaflet PVPE lipid was substantially faster; 3.252 (± 0.122) × 10^{-8} cm^2/s. Interestingly, the diffusion rate of the inner leaflet PVPE lipid was substantially faster than the corresponding lipid in a symmetrical bilayer which has a diffusion rate of 1.516 (± 0.294) × 10^{-8} cm^2/s (additional comparative diffusion rates are provided in the Supporting Information, Table S1).

Electroporation. The process of electroporation was studied by applying an external electric field of various strengths across the simulation cell.[13−17] A summary of the electroporation simulations and the time scales taken for electroporation events to occur is provided in table 3. Electroporation occurs within 200 ns for the higher electric field strengths of 0.5 and 0.4 V/nm, in both membranes. However, only the SaCM membrane is porated at the lowest field strength (0.3 V/nm) within the 200 ns time scale of the simulations. The detailed mechanisms of electroporation in the SaCM and EcOM membranes are discussed below for one typical simulation of each of the membranes to highlight the nature of the electroporation events in these two membranes.

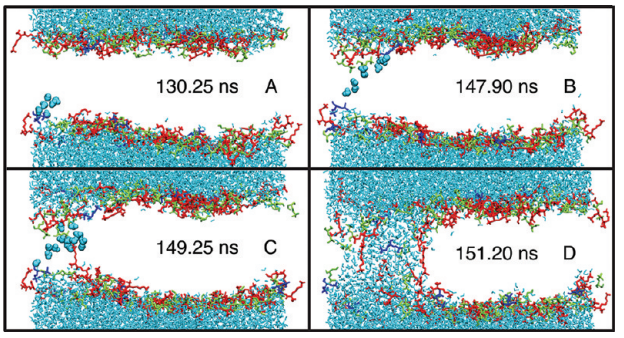

Figure 4. Typical sequence of events in the electroporation of the SaCM. This simulation was performed with an electric field of 0.3 V/nm applied. PG lipids are shown in green, Lys-PG in red, and DPG in blue. Lipid tails have been omitted for clarity.

S. aureus Cell Membrane. The mechanism of electroporation in the SaCM is similar to that previously determined for simpler membrane systems[12−18] (Figure 4). The first step in a typical membrane poration event is the formation of a defect in one of the leaflets of the membrane (Figure 4A). This defect is a point in the membrane where the head groups of a few (usually around three to five) lipids are located closer to the center of the bilayer than other "bulk" membrane lipids. This protrusion of the lipids toward the center of the bilayer is not due to a substantial alteration of the overall orientation of the head groups in the presence of the electric field (see Supporting Information, Figure S7A), but rather due to a local influence of the electric field in this part of the membrane. This defect is accompanied by the insertion of water molecules into the membrane at this point, with a stabilization of the water conformation due to interactions with the protruding lipid head groups. The next step in the mechanism of electroporation is the formation of a single-file water channel spanning the membrane. As the initial water channel forms, it is not accompanied by entry of lipid headgroups into the low dielectric region of the membrane (Figure 4B). As previously reported for simple bilayers, the formation of a membrane spanning water file is the event from which a pore will almost certainly then rapidly form in this membrane. Once the water channel has formed, lipid head groups are observed to move into the core of the membrane and to form hydrogen bonding interactions with the water molecules forming the channel (Figure 4C). The long headgroup of Lys-PG has a particular propensity to move into the core of the membrane to stabilize the water channel. This movement of Lys-PG, PG and DPG head groups disrupts the network of interactions that are usually present within the membrane, as new lipid−water interactions are formed to stabilize the channel. Once the lipids have moved to stabilize the water channel, the pore rapidly increases in size with phospholipids lining the pore (Figure 4D) until the membrane collapses. A snapshot of the system extracted from the early stages of pore formation, from 149.25 ns (Figure 4C), was used to initiate a simulation performed at the lower field strength of 0.04 V/nm. During this simulation the pore remained stable over the 100 ns (see Supporting Information, Figure 7B).

E. coli Outer Membrane. The electroporation of the asymmetric EcOM does not follow the same mechanism as the SaCM. The first step in the electroporation mechanism is, as in the case of the SaCM, the formation of a membrane defect. However, in all of the EcOM electroporation simulations the membrane

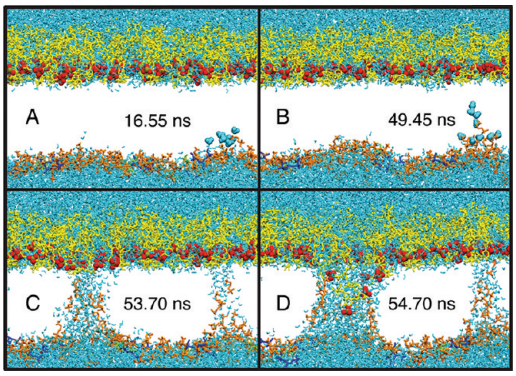

Figure 5. Typical sequence of events in the electroporation of the EcOM. This simulation was performed with an electric field of 0.4 V/nm applied. PE lipids are shown in orange, PG in green, DPG blue, and LPS in yellow. Lipid tails have been omitted for clarity.

defect is formed by the inner leaflet phospholipids, irrespective of the direction in which the electric field is applied (Figure 5A). Movement of water from the periplasmic side into the membranes accompanies the formation of defects in the inner leaflet. Subsequently, water molecules are able penetrate further into the core of the membrane (Figure 5B), where they form single-file water channels. In contrast to the electroporation of the SaCM, this does not always lead to rapid pore formation and disruption of the membrane, but rather these water channels are transient in nature. Most of the water molecules observed in the membrane were located within the inner leaflet where they are stabilized through hydrogen bonding interactions with the inner leaflet phospholipid head groups. For full poration to occur in the EcOM, inner leaflet phospholipids are required to move up into the core of the membrane to interact with water molecules in the outer leaflet of the membrane (Figure 5C). This interaction is often enabled through a flip-flopping of the inner leaflet phospholipids into the outer leaflet of the membrane. Only once a stable, phospholipid lined pore is formed, are LPS molecules able to move to line the pore (Figure 5D). This is followed by collapse of the membrane. To study the dynamics of the phospholipid-lined pore, a snapshot from 53.70 ns (Figure 5C) was extracted to initiate a simulation with an applied electric field strength of 0.04 V/nm. In contrast to the simulations of the SaCM pore, which remains stable throughout a 100 ns simulation, the phospholipid-lined pores of the EcOM collapse within 30 ns of the simulation to reform a defect-free membrane. During this collapse of the pore, inner leaflet phospholipids that have flip-flopped into the outer leaflet, can become trapped in the outer leaflet of the bilayer. Simulations performed at the higher electric field strength of 0.08 V/nm revealed a pore lined with phospholipids that was stable over 50 ns, however a second smaller pore was observed to collapse after 5 ns, this was followed by resealing of the membrane (see Supporting Information, Figure 7C).

DISCUSSION

Models of the EcOM and SaCM, developed in this work, were first validated through simulations performed of the individual membrane lipids. These model bilayer simulations confirm that the components of the membranes accurately reproduce experimental properties of these bilayers where available. The simulations of the pure Lys-DPPG bilayer also provide a prediction for the A_C of Lys-DPPG, which, to our knowledge, has yet to be determined experimentally.

Simulations of the SaCM bilayer, which capture the complexity of the headgroup and tail compositions of the "wildtype" SaCM, provide insights into the dynamics of this membrane at a resolution that has not previously been reported. First, it is likely that the anteiso-branched lipid tails are responsible for maintaining the membrane in the liquid crystal phase at a temperature of 313 K (this temperature is below the phase transition temperature for fully saturated 16 carbon PG and Lys-PG tails). Second, a complex pattern of intra- and intermolecular hydrogen bonding interactions is formed between the PG and Lys-PG lipid head groups, both of which lie roughly parallel to the bilayer plane throughout the simulations. This extended network of hydrogen bonding interactions provides a potential explanation for the experimental observation that the cationic antimicrobial peptide 6W-RP-1 binds to Lys-PG containing membranes but induces much reduced disruption compared to non-Lys-PG containing membranes.[59] It seems reasonable that hydrogen bonding interactions formed within the membrane, which include contributions from both ammonia groups of the Lys-PG headgroup, may inhibit the insertion of the peptide into the membrane.

The asymmetric model of the EcOM described above, accurately reproduces many experimentally determined properties of *E. coli* outer membranes. These include the A_C, association of divalent cations, hydrophobic thickness, and lipid diffusion. Encouragingly, the properties of the LPS molecules agree well with those determined from simulations of a *P. aeruginosa* outer membrane, despite differences in the structures of the LPS molecules, force fields and also simulation conditions used. Our simulations predict an increased in the diffusion rate of the EcOM inner leaflet lipids in comparison to the same lipids within a symmetric bilayer. This indicates that the LPS molecules in the outer leaflet of the asymmetric bilayer have an impact on the dynamics of the inner leaflet phospholipids. One possible explanation of this is that the very ordered nature of the LPS lipid tails allows reduced interdigitation of lipid tail, acyl chains between lipids of the opposite leaflets of the bilayer. Consequently, as the inner leaflet lipids interact less with the LPS molecules than they would with phospholipids, they are able to diffuse laterally within the monolayer at an increased rate.

A series of simulations were performed to explore the mechanisms of electroporation of the two bacterial membranes; key differences and similarities were observed. The set of simulations performed at differing electric field strengths, suggest that at the lower field strengths of 0.4 and 0.3 V/nm, the EcOM is more resistant to electroporation than the SaCM. The origins of the differences likely lie in the different mechanisms of electroporation of the two membranes. For the SaCM, the process of electroporation followed a similar pattern to that previously reported for model phospholipid membranes, that is, the initial formation of a water channel across the membrane followed by movement of lipids to line and stabilize the pore. The unique lipid composition of the SaCM facilitates this process; the shape and orientation of the Lys-PG lipids enables them to move into the membrane to stabilize the water channel during pore formation, with relative ease. Electroporation of the EcOM initially follows a similar mechanism; water molecules move into the bilayer to form channels across the membrane. However, as the bulky LPS molecules are unable to move into the core of the bilayer to stabilize the water channel, a large movement of the inner leaflet phospholipids is required, often through flip-flop of

the lipids, to stabilize the water channel. This movement of the inner leaflet lipids to interact with water molecules in the outer leaflet of the membrane appears to be the rate-determining step in pore formation. At lower electric field strengths, pores that had formed in the EcOM were observed to collapse, whereas pores in the SaCM remained stable over the course of these simulations.

CONCLUSIONS

In this work we have presented atomistic molecular dynamics simulations of two complex bacterial membranes: the outer membrane of Gram-negative bacterium *Escherichia coli* and the cell membrane of the Gram-positive bacterium *Staphylococcus aureus*. Our simulations reveal the extended intraleaflet interactions that stabilize both membranes. A series of simulations in which varying external electric fields were applied to the two membranes has provided an insight into their mechanisms of electroporation. The simulations have shown that the EcOM is more resistant to poration than the SaCM. The higher resistance to poration arises from the reduced mobility of LPS molecules such that phospholipids are required to stabilize the water-filled pore, resulting in some lipid flip-flop.

It is perhaps useful here to reflect on some methodological limitations of the present study. The relatively short time scales of the simulations do limit the amount of lipid motion we can observe within membranes, although electroporation has previously been studied via much shorter simulations. We have increased the sampling of our simulations by performing repeat calculations, in which the patterns of pore formation are retained. Furthermore, the diffusion rates of phospholipids match up well with experimentally determined values giving us confidence that the relative motion of the lipids within the two leaflets of the asymmetric EcOM are unable to stabilize the pore as efficiently as the symmetric leaflets of the SaCM.

The present simulations have demonstrated the utility of complex membrane models in studying the differences in the membranes of different bacterial species. In future work it will be of interest to explore the interactions of membrane proteins with detailed bacterial membranes. In this way it may be possible to identify and exploit the origins of the membrane-specific binding of antimicrobial peptides.

ASSOCIATED CONTENT

Supporting Information. Seven figures and six tables are provided. Methods of construction of the realistic membranes, details of the phospholipid, and LPS parameters and validation of the phospholipid parameters are also provided. This material is available free of charge via the Internet at http://pubs.acs.org.

AUTHOR INFORMATION

Corresponding Author

*E-mail: s.khalid@soton.ac.uk. Tel.: +44-2380-594176. Fax: +44-2380-593781.

ACKNOWLEDGMENT

This work was supported by a grant from the BBSRC (BB/H000658/1). S.K. is an RCUK fellow. We thank Tjerk Straatsma, Angel Piñeiro, Chris Neale, Joseph Goose, Mark Sansom and Peter Bond for helpful discussions and sharing of expertise. We also wish to acknowledge use of the IRIDIS High Performance Computing Facility at the University of Southampton.

ABBREVIATIONS

LPS, lipopolysaccharide; PE, phosphatidylethanolamine; PG, phosphatidylglycerol; Lys-PG, lysyl-phosphatidylglycerol; DPG, diphosphatidylglycerol (cardiolipin); PC, phosphatidylcholine; DM, 1,2-dimyristoyl; DP, 1,2-dipalmitoyl; PO, 1-palmitoyl, 2-oleoyl; PV, 1-palmitoyl, 2-cis-vaccenyl; POPO, 1-palmitoyl, 2-oleoyl, 3-palmitoyl, 4-oleoyl; PVPV, 1-palmitoyl, 2-cis-vaccenyl, 3-palmitoyl, 4-cis-vaccenyl; 15-a, Fifteen carbon anteiso-branched; EcOM, *Escherichia coli* outer membrane; SaCM, *Staphylococcus aureus* cell membrane; OMP, outer membrane protein; A_C, area per acyl chain; S_{CD}, deuterium order parameter; PME, particle mesh Ewald; MSD, mean squared displacement; CG, coarse-grained; MD, molecular dynamics; D_{HH}, headgroup-to-headgroup thickness

REFERENCES

(1) Osborn, M. J.; Rick, P. D.; Lehmann, V.; Rupprecht, E.; Singh, M. *Ann. N.Y. Acad. Sci.* **1974**, *235*, 52–65.
(2) Raetz, C. R. *Microbiol. Mol. Biol. Rev.* **1978**, *42*, 614–659.
(3) Osborn, M. J. *Annu. Rev. Biochem.* **1969**, *38*, 501–538.
(4) Qureshi, N.; Takayama, K.; Mascagni, P.; Honovich, J.; Wong, R.; Cotter, R. J. *J. Biol. Chem.* **1988**, *263*, 11971–11976.
(5) Raetz, C. R. H. *Annu. Rev. Biochem.* **1990**, *59*, 129–170.
(6) Sen, K.; Nikaido, H. *J. Bacteriol.* **1991**, *173*, 926–928.
(7) de Cock, H.; Brandenburg, K.; Wiese, A.; Holst, O.; Seydel, U. *J. Biol. Chem.* **1999**, *274*, 5114–5119.
(8) Wenzel, R. P.; Perl, T. M. *J. Hosp. Infect.* **1995**, *31*, 13–24.
(9) Haest, C. W. M.; De Gier, J.; Op Den Kamp, J. A. F.; Bartels, P.; Van Deenen, L. L. M. *Biochim. Biophys. Acta, Biomembr.* **1972**, *255*, 720–733.
(10) Roy, H. *IUBMB Life* **2009**, *61*, 940–953.
(11) Peschel, A.; Jack, R. W.; Otto, M.; Collins, L. V.; Staubitz, P.; Nicholson, G.; Kalbacher, H.; Nieuwenhuizen, W. F.; Jung, G.; Tarkowski, A.; et al. *J. Exp. Med.* **2001**, *193*, 1067–1076.
(12) Tieleman, D. P.; Leontiadou, H.; Mark, A. E.; Marrink, S.-J. *J. Am. Chem. Soc.* **2003**, *125*, 6382–6383.
(13) Tieleman, D. P. *BMC Biochem.* **2004**, *5*, 10.
(14) Tarek, M. *Biophys. J.* **2005**, *88*, 4045–4053.
(15) Vernier, P. T.; Ziegler, M. J. *J. Phys. Chem. B* **2007**, *111*, 12993–12996.
(16) Ziegler, M. J.; Vernier, P. T. *J. Phys. Chem. B* **2008**, *112*, 13588–13596.
(17) Böckmann, R. A.; de Groot, B. L.; Kakorin, S.; Neumann, E.; Grubmüller, H. *Biophys. J.* **2008**, *95*, 1837–1850.
(18) Sun, S.; Yin, G.; Lee, Y.-K.; Wong, J. T. Y.; Zhang, T.-Y. *Biochem. Biophys. Res. Commun.* **2011**, *404*, 684–688.
(19) Vernier, P. T.; Ziegler, M. J.; Sun, Y.; Chang, W. V.; Gundersen, M. A.; Tieleman, D. P. *J. Am. Chem. Soc.* **2006**, *128*, 6288–6289.
(20) Fernández, M. L.; Marshall, G.; Sagués, F.; Reigada, R. *J. Phys. Chem. B* **2010**, *114*, 6855–6865.
(21) Khalid, S.; Sansom, M. S. P. *Mol. Membr. Biol.* **2006**, *23*, 499–508.
(22) Khalid, S.; Bond, P. J.; Deol, S. S.; Sansom, M. S. P. *Proteins* **2006**, *63*, 6–15.
(23) Khalid, S.; Bond, P. J.; Carpenter, T.; Sansom, M. S. P. *Biochim. Biophys. Acta, Biomembr.* **2008**, *1778*, 1871–1880.
(24) Gumbart, J.; Wiener, M. C.; Tajkhorshid, E. *J. Mol. Biol.* **2009**, *393*, 1129–1142.
(25) Lins, R. D.; Straatsma, T. P. *Biophys. J.* **2001**, *81*, 1037–1046.
(26) Shroll, R. M.; Straatsma, T. P. *Biopolymers* **2002**, *65*, 395–407.
(27) Lins, R. D.; Vorpagel, E. R.; Guglielmi, M.; Straatsma, T. P. *Biomacromolecules* **2007**, *9*, 29–35.
(28) Soares, T. A.; Straatsma, T. P. *Mol. Simul.* **2008**, *34*, 295–307.
(29) Gould, R. M.; Lennarz, W. J. *J. Bacteriol.* **1970**, *104*, 1135–1144.
(30) White, D. C.; Frerman, F. E. *J. Bacteriol.* **1968**, *95*, 2198–2209.

(31) Vinogradov, E. V.; van der Drift, K.; Thomas-Oates, J. E.; Meshkov, S.; Brade, H.; Holst, O. *Eur. J. Biochem.* **1999**, *261*, 629–639.
(32) Appelmelk, B. J.; An, Y.; Hekker, T. A. M.; Thijs, L. G.; MacLaren, D. M.; de Graaf, J. *Microbiology* **1994**, *140*, 1119–1124.
(33) Lugtenberg, E. J. J.; Peters, R. *Biochim. Biophys. Acta, Lipid Lipid Met.* **1976**, *441*, 38–47.
(34) Berendsen, H. J. C.; van der Spoel, D.; van Drunen, R. *Comput. Phys. Commun.* **1995**, *91*, 43–56.
(35) van der Spoel, D.; Lindahl, E.; Hess, B.; Groenhof, G.; Mark, A. E.; Berendsen, H. J. C. *J. Comput. Chem.* **2005**, *26*, 1701–1718.
(36) Hess, B.; Kutzner, C.; van der Spoel, D.; Lindahl, E. *J. Chem. Theory Comput.* **2008**, *4*, 435–447.
(37) Oostenbrink, C.; Villa, A.; Mark, A. E.; Van Gunsteren, W. F. *J. Comput. Chem.* **2004**, *25*, 1656–1676.
(38) Berendsen, H.; Postma, J.; van Gunsteren, W.; Hermans, J. Interaction Models for Water in Relation to Protein Hydration. In *Intermolecular Forces*; Pullman, B., Ed.; D. Reidel Publishing Company: Boston, MA, 1981; pp 331−342.
(39) Emmerling, G.; Henning, U.; Gulik-Krzywicki, T. *Eur. J. Biochem.* **1977**, *78*, 503–509.
(40) Van Alphen, L.; Lugtenberg, B.; Rietschel, E. T.; Mombers, C. *Eur. J. Biochem.* **1979**, *101*, 571–579.
(41) Brandenburg, K.; Seydel, U. *Biochim. Biophys. Acta, Biomembr.* **1984**, *775*, 225–238.
(42) Brandenburg, K.; Funari, S. S.; Koch, M. H. J.; Seydel, U. *J. Struct. Biol.* **1999**, *128*, 175–186.
(43) Danner, S.; Pabst, G.; Lohner, K.; Hickel, A. *Biophys. J.* **2008**, *94*, 2150–2159.
(44) Overath, P.; Traeuble, H. *Biochemistry* **1973**, *12*, 2625–2634.
(45) Nosé, S. *Mol. Phys.* **1984**, *52*, 255–268.
(46) Hoover, W. G. *Phys. Rev. A* **1985**, *31*, 1695.
(47) Parrinello, M.; Rahman, A. *J. Appl. Phys.* **1981**, *52*, 7182–7190.
(48) Nosé, S.; Klein, M. L. *Mol. Phys.* **1983**, *50*, 1055–1076.
(49) Essmann, U.; Perera, L.; Berkowitz, M.; Darden, T.; Lee, H.; Pedersen, L. *J. Chem. Phys.* **1995**, *103*, 8577–8593.
(50) Hess, B. *J. Chem. Theory Comput.* **2007**, *4*, 116–122.
(51) Kukol, A. *J. Chem. Theory Comput.* **2009**, *5*, 615–626.
(52) Petrache, H. I.; Dodd, S. W.; Brown, M. F. *Biophys. J.* **2000**, *79*, 3172–3192.
(53) Kannenberg, E.; Blume, A.; McElhaney, R. N.; Poralla, K. *Biochim. Biophys. Acta, Biomembr.* **1983**, *733*, 111–116.
(54) Zhao, W.; Róg, T.; Gurtovenko, A. A.; Vattulainen, I.; Karttunen, M. *Biophys. J.* **2007**, *92*, 1114–1124.
(55) Snyder, S.; Kim, D.; McIntosh, T. J. *Biochemistry* **1999**, *38*, 10758–10767.
(56) O'Keeffe, A. H.; East, J. M.; Lee, A. G. *Biophys. J.* **2000**, *79*, 2066–2074.
(57) Kučerka, N.; Tristram-Nagle, S.; Nagle, J. *J. Membr. Biol.* **2006**, *208*, 193–202.
(58) Schindler, M.; Osborn, M. J.; Koppel, D. E. *Nature* **1980**, *283*, 346–350.
(59) Kilelee, E.; Pokorny, A.; Yeaman, M. R.; Bayer, A. S. *Antimicrob. Agents Chemother.* **2010**, AAC.00191–00110.